Microfluidic dissolution of nanoemulsions in solvents

Thai Dinh¹, Yixuan Xu², Thomas G. Mason^{3,4}, and Thomas Cubaud^{1*}

¹Department of Mechanical Engineering, Stony Brook University, Stony Brook, NY 11794 USA

²Department of Materials Science and Engineering, University of California- Los Angeles, Los Angeles, CA 90095 USA

³Department of Chemistry and Biochemistry, University of California- Los Angeles, Los Angeles, CA 90095 USA

⁴Department of Physics and Astronomy, University of California- Los Angeles, Los Angeles, CA 90095 USA

Abstract

We experimentally investigate the behavior of nanoemulsion and microscale emulsion jets flowing in solvents using coaxial microfluidic devices. The stability of colloidal dispersions made of oil droplets dispersed in water is significantly altered by the presence of a miscible solvent, which induces complex solutal and droplet coalescence instabilities over various time-scales. We reveal intriguing microflow patterns of oil-in-water micro- and nanoemulsion threads in a continuous phase of isopropanol, including the dissolving, diffusive, gravitational, and stable thread regimes. We discuss the evolution of core-annular flow characteristics and develop scaling relationships to model thread dynamics through measurements of effective diameter as well as persistence and gravitational lengths. A microflow method based on dynamic similitude is developed to estimate the diffusion coefficients of nanoemulsions and microscale emulsions in miscible solvents. This work shows the possibility to process soft colloidal dispersions and control degradation mechanisms using microfluidic techniques.

1

^{*} Email: Thomas.cubaud@stonybrook.edu

1. Introduction

The stability of fine fluid dispersions with respect to contaminants is important to the processing of colloids in a variety of contexts, including in the food, cosmetic, printing, and pharmaceutical industries, as well as in the environmental and energy sectors. The possibility to make and unmake colloidal fluid dispersions at will is appealing; however, while significant efforts have been devoted to understand the formation of micro- and nanoscale emulsions better using various flow processing techniques, 1-3 few studies have addressed flow destabilization processes associated with the addition of solvents at such a small scale. 4-6. In recent years, the field of nanoemulsion science has gained expanding interest due to the high-throughput capabilities of nanoemulsion production with tunable average droplet radii ranging from 5 nm to 100 nm; such nanoemulsions can have long shelf lives.⁷ Despite their simple composition, including two immiscible phases, such as oil and water, and a surfactant to stabilize droplets against coalescence, nanoemulsions display complex rheological and optical behavior. ⁷ Depending on the hydrophile-lipophile balance of surfactant, oil-in-water (O/W) or water-in-oil (W/O) emulsions are produced using either low-energy emulsification techniques with the adjunction of a co-surfactant, 8-10 or highenergy emulsification methods, such as high-shear homogenizer and ultrasonication. 11-13 The advantages of the high-shear homogenizer method consists in the possibility to reach very small droplet sizes with a high degree of monodispersity and the absence of co-surfactant, thereby creating a simple model colloidal fluid. Hence, it would be useful to probe the microflow behavior of simple nanoemulsions with a solvent, which is miscible in both phases, in order to refine our understanding of interfacial and diffusive flow properties of colloids in confined environments and to dynamically manipulate emulsion and solvent interactions, such as nanoscale droplet coalescence processes, for advanced material synthesis.

Microfluidic devices enable unique control of fluids at the micro and sub-microscale with low input volume and over a wide range of flow rates and geometries. ¹⁴⁻¹⁸ The ability to control streams at a small scale facilitates the formation of steady multiphase flows of droplets and the generation of fine-tune emulsions in porous-like media using a variety of fluid contactors, including hydrodynamic focusing sections, T-junctions, and centerline injections. ¹⁹⁻²⁷ The size of droplets generated on chip, however, typically scales with the channel width and remains on the order of a few micrometers, which is much larger than the size of nanoemulsion droplets. As a result, examining the influence of chemical additives on the stability of dispersions made on chip is limited to a few channel-to-droplet size ratios. Hence, there is a need for developing model studies with well-characterized nanoemulsions to elucidate the microflow phenomenology associated with the transport of colloids with solvent in porous-like media at very large channel-to-droplet size ratios. In addition to the formation of dispersions, microfluidic devices are also practical for forming separated flows, such as threads and jets, *i.e.*, core-annular flows, ²⁸⁻³² which enables independent control of fluid interfacial area and residence time, and are therefore useful in applications such as micromixing and fiber synthesis. ³³⁻³⁸ Threads, however are prone to numerous

physicochemical hydrodynamic instabilities³⁹⁻⁴¹ and little is known about the stability of nanoemulsion threads in miscible solvents at small scales relevant for microfluidics.

Here, we examine the dynamic behavior of micro- and nano-scale O/W emulsions flowing in isopropanol solvent using coaxial microfluidic devices. Well-characterized emulsions, which are made of silicone oils and aqueous solutions of sodium dodecyl sulfate (SDS) are chosen as model fluids due to the simplicity and widespread use of their components. Similarly, isopropyl alcohol is selected as a solvent due to its miscibility with both water and silicone oil, low toxicity, and extensive use in common laboratory and industrial operations. While blends of isopropanol and aqueous solution of SDS, as well as blends of isopropanol and silicone oil fully mix in a vial and do not separate over time, ternary systems made of water, oil, and solvent display more complex behavior, including changes of optical properties and droplet coalescence depending on the relative proportion of each component. In particular, nanoemulsions and isopropanol are found to mix at large solvent concentrations and phase separate at moderate to low solvent concentrations. Hence, to clarify the microscale interactions of nanoemulsion and solvent at short time scales, i.e., far from thermodynamic equilibrium, an emulsion thread is formed in a sheath of solvent through injection of the colloid in a microneedle, which is aligned along the centerline of a square glass microcapillary tube with solvent infusing. This method permits independent control of flow rates, and the use of borosilicate glass microcells provides excellent chemical resistance and enables flow visualization from all sides of the device. In particular, we employ a flow-based method to study nanoemulsion threadsolvent interactions at different time-scales and we examine the role of flow rates and microchannel orientation on the behavior of core-annular flows made of nanoemulsion threads in an external phase of solvent. A variety of flow arrangements are uncovered, including dissolving, diffusive, gravitational, and stable thread regimes. The stable regime corresponds to the situation where convection is dominant over solvent diffusion and tread morphology is well predicted with hydrodynamic theory. By contrast, the dissolving regime is characterized by an apparent melting of emulsion threads in the solvent phase at low flow rates. At intermediate velocities, the flow rate-modulated gravitational and diffusive thread regimes are found to depend on the average properties of emulsions, such as density and diffusion. A systematic study of thread dynamics is conducted to elucidate the role of convection and diffusion on dissolving colloidal emulsions and to better characterize individual flow regime and their transitions. A microfluidic method is developed to estimate the effective diffusion coefficient of colloidal emulsions treated as monophasic fluids with solvent based on dynamic similitude. We also discuss intricate flow morphology and document the evolution of droplet coalescence processes along the flow direction.

2. Experimental Methods

2.1. Emulsion preparation

Highly monodisperse colloidal dispersions of oil droplets in water are produced using several preparation stages as illustrated in Fig. 1(a). First, a silicone oil of kinematic viscosity *v* and an aqueous solution of sodium dodecyl

sulfate (SDS) at a concentration 10 mM, which is in slight excess of the critical micelle concentration (CMC) of 8 mM to ensure nanodroplets coverage and obtain a constant interfacial tension $\gamma \approx 12$ mN/m, are dispersed using a stirrer at large speed to form a premixed emulsion, which is then size-fractionated using multiple ultracentrifuge steps to form a concentrated macroscale emulsion having a monodisperse oil droplet distribution with an average droplet radius $\langle a \rangle \sim 10^{-6}$ m. A significant reduction of the droplet size is obtained through multiple passes of the macroscale emulsion in a microfluidic homogenizer at extreme shear rate⁷ to obtain a very fine colloidal dispersion, which in turn is size-fractionated using various ultracentrifuge steps to form a uniform nanoemulsion having $\langle a \rangle$ ranging between 10^{-8} and 10^{-7} m. In this work, we investigate the microflow behavior of two dispersions made using this method, including (a) a nanoemulsion, which is passed eight times at 3×10⁴ psi in a homogenizer and comprised of polydimethylsiloxane oil of viscosity v = 10 cSt with a droplet size $\langle a \rangle = 51$ nm and an initial concentration of $\Phi = 0.564$, and (b) a microscale emulsion, which is passed five times at 1×10^4 psi in a homogenizer and composed of silicone oil of viscosity v = 350 cSt with a droplet size of $\langle a \rangle = 0.58$ μ m and initial concentration of $\Phi = 0.778$. These emulsions are subsequently diluted in a 10 mM agueous solution of SDS well below the nanodroplet jamming point before being introduced in the centerline injection of a coaxial microchannel [Fig. 1(b)]. As a result, the final volume fraction for the nanoemulsion is $\Phi = 0.17$ with a density of $\rho = 1.04$ g/mL and the final volume fraction for the microscale emulsion is $\Phi = 0.36$ with a density of $\rho = 1.03$ g/mL. The dynamic viscosity of the diluted emulsions is measured using a falling ball viscometer and estimated at 24.9 cP for the nanoemulsion and 20.4 cP for the microscale emulsion.

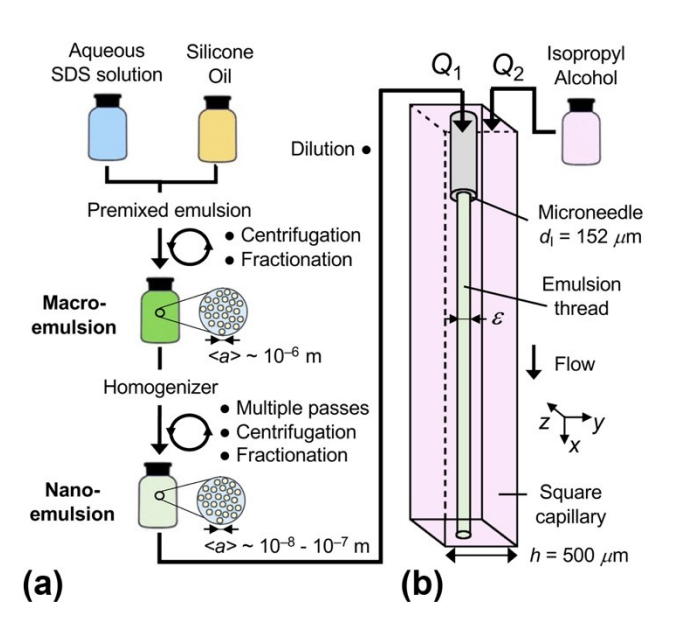


Fig. 1 Diagram of the experimental method with schematics of (a) emulsion preparation steps and (b) downward central injection of nanoemulsion (fluid L1) at flow rate Q_1 in a solvent (fluid L2) flowing at Q_2 using a coaxial microchannel.

2.2. Coaxial Microchannel

We utilize coaxial microfluidic devices to analyze the behavior of O/W emulsion jets in a sheathing flow of high purity isopropyl alcohol (ACS reagent, $\geq 99.5\%$) having dynamic viscosity of 2.2 cP and density of 0.785 g/mL. The microchannel is made of a square capillary tube having internal width $h = 500 \mu m$ in which a cylindrical microneedle, having an outer diameter $d_0 = 305 \mu m$ and inner diameter $d_1 = 152 \mu m$, is centrally encased. The microneedle is made of stainless steel with a blunt flat tip and used to inject the nanoemulsion (fluid L1) at flow rate Q_1 into the main channel where the solvent (fluid L2) is flowing along the x-direction of the channel at flow rate Q_2 . [Fig. 1(b)]. The microfluidic device is mounted into a frame where two cameras equipped with high-magnifying lenses are positioned to visualize microflows both in the y- and z-planes. A micro-stage is attached to the device outlet to precisely align the microneedle along the microchannel centerline with the help of the two cameras. Fluids are injected into the device using syringe pumps and gas-tight syringes. Our versatile experimental apparatus enables investigations of multiphase microflow behaviors in various conditions, including horizontal, upward, and downward orientations.

2.3. Stable threads

An advantage of coaxial microchannels resides in the direct formation of simple core-annular flows through the introduction of nanoemulsion in the centerline injector at volumetric flow rate Q_1 and the infusion of solvent in the main channel at Q_2 . A useful method of analysis consists in examining the role of flow rates based on the total rate $Q_T = Q_1 + Q_2$, which sets thread convective time-scales, and the flow rate ratio $\varphi = Q_1/Q_2$, which controls the thread diameter ε . For large viscosity contrasts $\chi = \eta_1/\eta_2 \gg 1$ and neglecting molecular diffusion and interfacial tension,⁴² the normalized thread diameter ε_0/h in circular capillaries is simply derived from Stokes equations⁴³ and modeled as:

$$\frac{\varepsilon_0}{h} = \left(\frac{\varphi}{2+\varphi}\right)^{1/2},\tag{1}$$

which is independent of Q_T . Previous work⁴⁴ on the behavior of viscous threads made of simple silicone oils in square microchannels has shown good agreement with eqn (1).

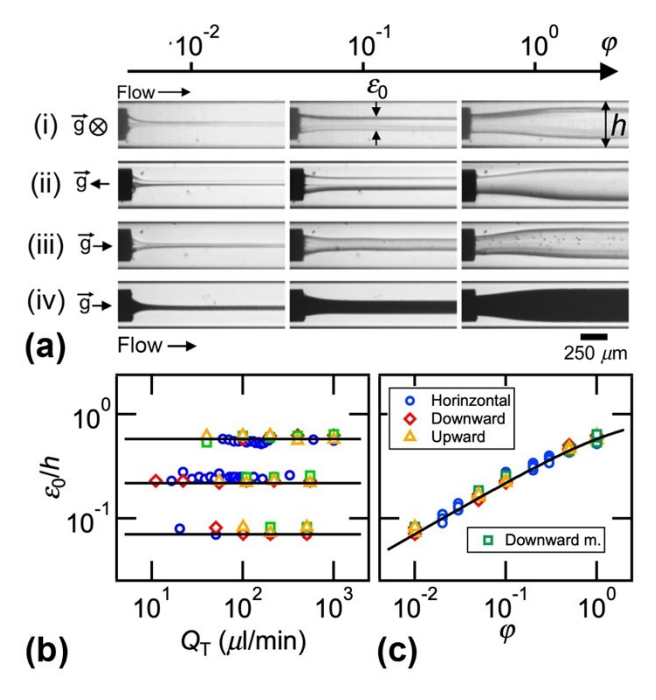


Fig. 2 (a) Micrographs of stable threads in various channel orientations at flow rate ratios $\varphi = 10^{-2}$, 10^{-1} , and 1. (i) Horizontal, (ii) upward, and (iii) downward injection of nanoemulsion in isopropanol. (iv) Downward injection of microscale emulsion in solvent. The thread appears dark due to strong multiple scattering of illuminating visible light. (b) Normalized thread diameter ε_0/h as a function of Q_T for $\varphi = 10^{-2}$, 10^{-1} , and 1. (c) Measurements of stable ε_0/h as a function of φ for all fluid pairs and channel orientations. Solid line: eqn (1).

Here, we experimentally measure the width \mathscr{E}/h of threads made of nanoemulsion and microscale emulsion in a sheath of isopropanol near the fluid junction at large Q_T , *i.e.*, at high flow velocity where diffusive phenomena are negligible (Fig. 2). As can be seen from micrographs at various orientations, the thread size ε reaches a constant width ε_0 in the main channel with various optical properties for the emulsions [Fig. 2(a)]. Experiments conducted at fixed φ and varying Q_T show that measurements of ε/h are comparable to the stable thread diameter ε_0/h , which remains independent of Q_T [Fig. 2(b)]. Overall, for φ ranging between 10^{-2} and 1, data show good agreement with eqn (1) for all channel orientations and fluid pairs [Fig. 2(c)]. This property is useful for the study of thread dissolution processes as it provides a reference length scale. In the following, we investigate thread behavior at fixed values of the flow rate ratio φ and vary the total flow rate Q_T to characterize threads based on their stable size. In particular, we examine the role of flow velocity on the evolution of diffusive flow characteristics of nanoemulsion threads in isopropanol along iso- φ curves. Wide variations of flow rates enable the crossover between numerous flow regimes of interest, including the dissolving, diffusive, gravitational, and stable thread regimes.

3. Flow Regimes

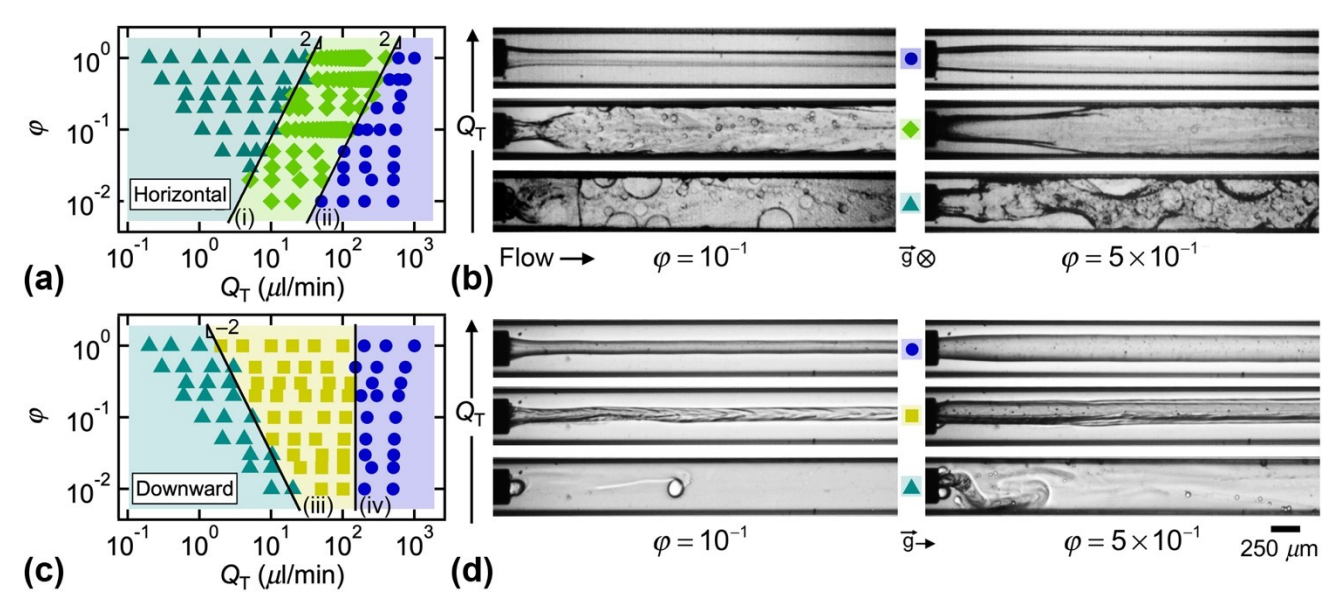


Fig. 3 Typical nanoemulsion-in-solvent flow patterns in coaxial microchannels for horizontal and downward orientations, flow rates in μ l/min. (a) Horizontal configuration: phase-diagram of flow rate ratio φ as a function of total flow rate Q_T , including dissolving (\triangle), gravitational (\diamondsuit), and stable thread (\spadesuit) regimes. Solid lines: (i) $\varphi = (Q_T/35.7)^2$ and (ii) $\varphi = (Q_T/447.2)^2$. (b) Micrographs for horizontal injection at fixed φ and varying Q_T . Left: $\varphi = 10^{-1}$ and $Q_T = 5.5$, 22, and 550. Right: $\varphi = 5 \times 0^{-1}$, $Q_T = 30$, 75, and 750. (b) Downward configuration: $\varphi - Q_T$ phase-diagram, including dissolving (\triangle), diffusive (\blacksquare), and stable thread (\spadesuit) regimes. Solid lines: (iii) $\varphi = (Q_T/1.8)^{-2}$ and (iv) $Q_T = 150$. (d) Micrograph of downward injection. Left: $\varphi = 10^{-1}$ and $Q_T = 1.1$, 55, and 550. Right: $\varphi = 5 \times 10^{-1}$ and $Q_T = 1.5$, 6, and 750.

The introduction of oil-in-water nanoemulsion in miscible solvent at the small scale presents various flow regimes depending on flow rates of injection Q_1 and Q_2 and microchannel orientations [Fig. 3]. While for both horizontal and vertical orientations, stable threads are observed at large total flow rates Q_T , flow regimes differ at moderate Q_T with the presence of a gravitational regime, characterized by the fall of threads toward the bottom wall and the formation of layered-flows, in the horizontal case [Figs. 3(a) and 3(b)] and the appearance of a diffusive regime, in which the thread is seen to progressively swell along the flow direction, in the vertical situation [Figs. 3(c) and 3(d)]. At low rates of injection Q_T , complex dissolution patterns are observed with the emergence of small oil droplets resulting from a series of stochastic coalescence-induced processes enabled by the diffusion of the solvent in both the water and oil phases of the nanoemulsion. Hence, the dissolving regime is defined by the erosion of nanoemulsion threads in the field of view, *i.e.*, for x/h ranging between 0 and 10, with the resulting complex solutal convection, Marangoni flows, and wetting phenomena observed near the fluid contactor. In the horizontal configuration, sessile droplets are seen to accumulate at the channel walls producing slowly evolving complex flow paths [Fig. 3(b)]. By contrast, in the downward configuration, nanoemulsion threads rapidly dissolve at the fluid contactor with the development of intriguing flow structures [Fig. 3(d)]. Whereas typical flow patterns present

similarities for both channel orientation, functional relationships delineating flow regimes, however, significantly differ as transition curves scale as $\varphi \sim Q_T^2$ for horizontal channels [Fig. 3(a)] and as $\varphi \sim Q_T^{-2}$ for the dissolving/diffusive transition of vertical channels [Fig. 3(c)]. The transition to stable threads is found at constant Q_T in the vertical case [Figure 3(d)] indicating that the diffusive regime, which is characterized by an enlargement of the effective thread diameter along the flow direction, corresponds to a convective instability where perturbations are carried away with the flow. This effect is observed in vertical channels due to the absence of significant fluid density-based gravitational drift, which in horizontal channels leads to the thread contact with the bottom walls at distance L_G from the needle.

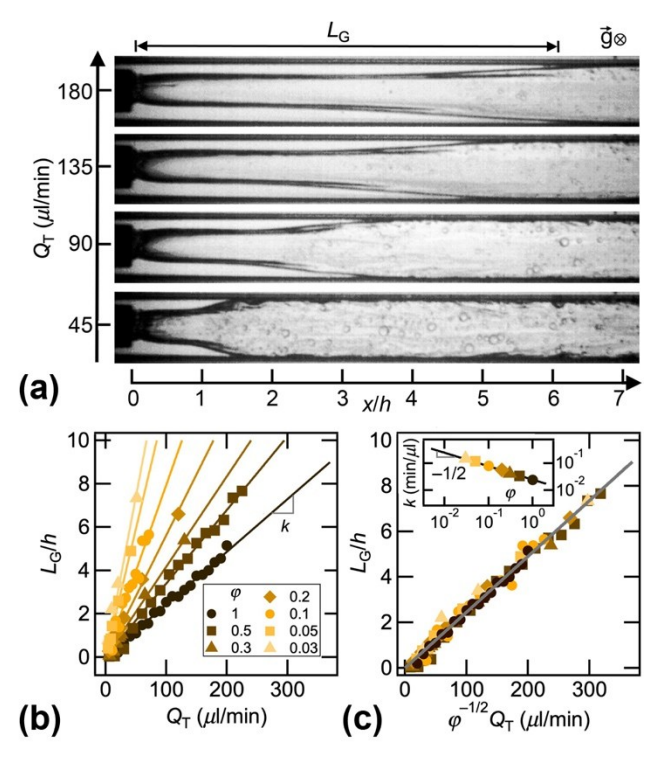


Fig. 4 Horizontal configuration. (a) Micrographs of flow patterns in the gravitational regime for fixed $\varphi = 0.5$ and varying $Q_{\rm T}$ showing the growth of the gravitational length $L_{\rm G}$ with $Q_{\rm T}$. (b) Evolution of normalized length $L_{\rm G}/h$ along iso- φ lines as a function of $Q_{\rm T}$. Solid lines: $L_{\rm G}/h = kQ_{\rm T}$. (c) Gravitational length $L_{\rm G}/h$ vs. $\varphi^{-1/2}Q_{\rm T}$ for all φ . Solid line: Eq. (2). Inset: Evolution of prefactor k with flow rate ratio φ . Solid line: $k = 2 \times 10^{-2} \varphi^{-1/2} \min/\mu l$.

Our previous work on nanoemulsion thread stability in horizontal channels⁴¹ has examined the side-view features of the gravitational regime as a function of density differences $(\rho_1 - \rho_2)/\rho_1$ and characterized the evolution of the thread centerline inclination with Q_T^{-1} . It was shown in particular that the gravitational length – defined as the distance between the microneedle and the points of contact of the thread with the walls – scales as $L_G \sim Q_T$. Here, we employ a similar approach and directly measure L_G from micrographs [Fig. 4(a)] and show that for a given φ , the gravitational length L_G varies linearly with Q_T according to a restricted homogeneous equation L_G/h

= kQ_T [Fig. 4(b)]. The dimensional factor k is determined for each φ and is well fitted by a function of the form of $k = 2 \times 10^{-2} \varphi^{-1/2}$ min/ μ l [Fig. 4(c)-inset]. This finding is incorporated into the master curve $L_G/h = 2 \times 10^{-2} \varphi^{-1/2}Q_T$ [Fig. 3(c)]. Hence, the gravitational length is expressed using a general homogeneous equation, such as

$$\frac{L_G}{h} = \varphi^{-1/2} \frac{Q_T}{Q_G}, \tag{2}$$

where $Q_G = 50 \ \mu l/min$. In horizontal case, tiny droplets appear around points of contact between the thread and the wall thereby indicating local dissolution of nanoemulsion through series of droplet coalescence in low velocity regions. In addition, the deceleration of envelope of inner fluid L1 when it reaches the channel wall, at gravitational length L_G , facilitates the diffusion of emulsion and solvent in low fluid mobility regions. The fouling of the bottom channel wall and the formation of sheared stratifications for $x/h \ge L_G/h$, however, reduce the specific interfacial area between nanoemulsion and solvent and does not present notable advantages to enhance mixing compared to core annular flows. Overall, the scaling $L_G/h \sim Q_T \varphi^{-1/2}$ is in good agreement with flow maps [Fig. 3(a)] for predicting flow transitions since assuming a constant $L_G/h \sim 10$ at the stable thread transition yields a scaling $\varphi \sim Q_T^2$. In this case, both transitions on the horizontal flow map are well fit with a function of the type

$$\varphi_{\rm C, H} = \left(\frac{Q_{\rm T}}{Q_{\rm H}}\right)^2,\tag{3}$$

where $Q_{\rm H} = 35.7~\mu$ l/min for the dissolving thread/gravitational regime transition and $Q_{\rm H} = 447.2~\mu$ l/min for the gravitational/stable thread transition.

A useful feature of the vertical configuration consists in the formation of threads having no significant gravitational drift toward the channel walls, which permits to decorrelate diffusive from gravitational effects at low velocities and access intriguing flow regimes dominated by dissolution. To further characterize vertical configurations, we also investigate the upward flow of nanoemulsions and find that, beside slight variations in flow morphologies, the associated flow map is very similar to the downward case with transition lines defined as

$$\varphi_{\text{C,V}} = \left(\frac{Q_{\text{T}}}{Q_{\text{V}}}\right)^{-2},\tag{4}$$

with $Q_V = Q_{V,N} = 1.8 \ \mu\text{l/min}$, for the dissolution/diffusive regime transition and a stable thread transition occurring at fixed value of $Q_T = 150 \ \mu\text{l/min}$ [Fig. 5(a)]. Hence, data suggest the critical flow rate $Q_{V,N}$ used to normalize Q_T is related to the diffusive properties of the nanoemulsion and solvent combination. As the diffusion velocity J between thread and solvent depends on diffusion coefficient D and concentration gradient according to Fick's law,⁴⁵ we assume that the diffusion flow rate $Q_D = JA$, where A is the thread surface area $A = \pi \varepsilon L_P$ and L_P is the thread length, remains constant at the flow transition. This argument leads to $Q_D/A \sim Q_T/h^2$ for the diffusion and flow velocities, hence the critical flow rate is expected to scale as $Q_T \sim \varphi^{-1//2} L_P^{-1}$ since $\varepsilon \sim \varphi^{1/2}$ for small threads.

The transition between dissolving and diffusive regimes is observed over a fixed field view, such as $L_P \sim 10h$. Therefore, curves of the form $\varphi \sim Q_T^{-2}$ are found to delineate flow patterns on experimental flow maps.

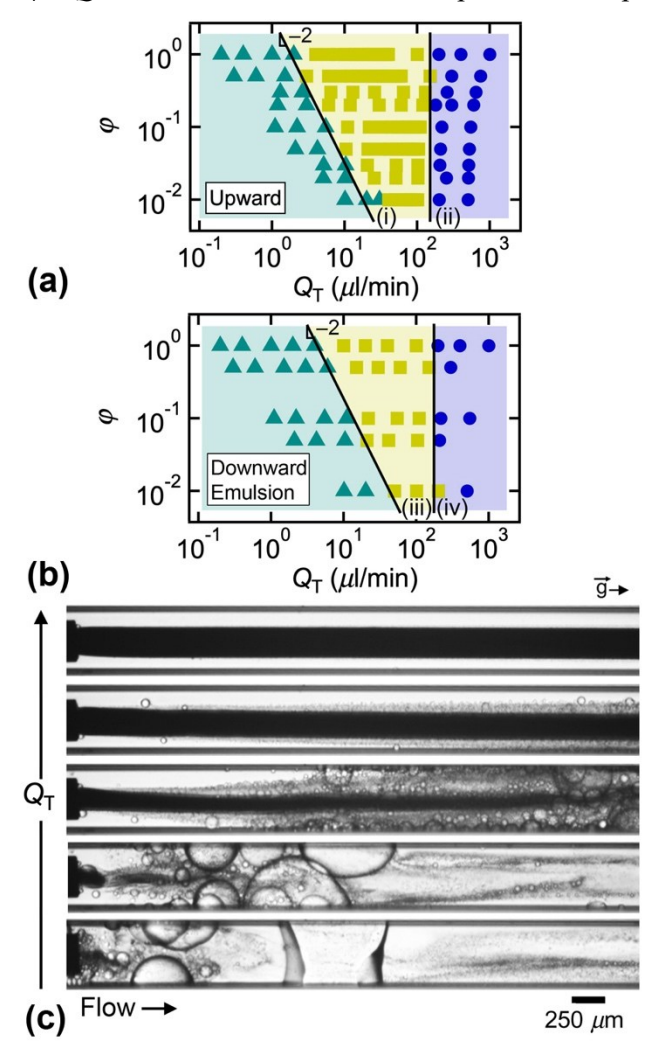


Fig. 5 Vertical configuration. Flow rates in μ l/min. (a) Flow map of upward injection of nanoemulsion. Solid lines: (i) $\varphi = (Q_T/1.8)^{-2}$, (ii) $Q_T = 150$. (b) Flow map of downward configuration with microscale emulsion. Solid lines: (iii) $\varphi = (Q_T/4.3)^{-2}$, (iv) $Q_T = 150$. (c) Micrographs of flow patterns corresponding to (b) at fixed $\varphi = 5 \times 10^{-1}$ and $Q_T = 0.3$, 0.6, 6, 30, and 300 (from bottom to top)

To further examine the relationship between critical flow rates and fluid properties, we also examine the microfluidic behavior of microscale emulsion and solvent in the downward configuration and find a similar flow map as with the nanoemulsion but with a shift in the dissolving/diffusive transition defined by $\varphi = (Q_T/Q_V)^{-2}$, with $Q_{V,E} = 4.3 \ \mu\text{l/min}$ [Fig. 5(b)]. While directly relating the absolute values of critical flow rates Q_V found in flow maps to fluid diffusion coefficients D is not evident, correlating flow rates and diffusion coefficient such as $Q_V \sim$

D suggests the ratio $Q_{V,E}/Q_{V,N} \approx 2.4$ also corresponds to the ratio of their effective diffusion coefficient D_E/D_N during solvation of O/W emulsions having various < a >.

Flow regimes obtained with the microscale emulsion resemble those of the nanoemulsion. There are, however, significant differences in optical properties due to large variation in average droplet size $\langle a \rangle$ and concentration Φ . In particular, the jet of microscale emulsion appears opaque (*i.e.* very dark as a consequence of strong multiple scattering, thereby reducing transmitted light) in our microfluidic apparatus [Fig. 5(c)]. As a result, the sharper contrast between the colloid and the solvent reveals the complex structure of the dissolution regime with metastable formation of sessile drops of dissolved material at the walls and the apparent melting of the emulsion thread at a certain distance x/h from the injection needle at low Q_T . The diffusive regime is characterized by a thread traversing the initial field of view and the distribution of fine droplets at the walls indicating the width of active diffusion processes, which can be measured as ε/h at intermediate Q_T . The stable thread regime is commonly encountered at larger Q_T . Measurement of key features, such as the thread persistence length in the dissolution regime and the downstream thread width in the diffusive regime, offer the possibility for quantitative analysis of thread alteration processes.

4. Dissolution of Emulsion Threads

In this section, we examine the morphology and dynamics of dissolving and diffusive threads in the downward configuration, when gravitational effects are not expected to significantly influence fluid interplay. As the solvent progressively diffuses into the aqueous continuous phase, dispersed oil droplets undergo a series of complex dissolution and recombination processes, including growth and coalescence, which ultimately lead to the formation of much larger droplets slowly moving at the walls at low Q_T [Fig. 6(a)]. The opacity of the emulsion with large <a> makes it practical to reveal the thread spatial evolution and makes it apparent that tiny droplets emerge from the central stream, which is not in contact with the channel walls, after a certain distance from microneedle tip. As for low Q_T , the thread laterally spreads and becomes more transparent in region of wetting droplets, the downstream flow consists of complex heterogeneous mixtures and we define a thread persistence length L_P to characterize the thread ability to maintain structural integrity. We experimentally measure L_P in the field of view from micrographs through analysis of light intensity per channel width along the flow direction for specific flow rate ratios φ as a function of the total flow rate Q_T [Fig. 6(b)]. Curves of iso- φ are found to scale as a restricted homogeneous equation $L_P/h \sim kQ_T^{2/3}$, where the dimensional prefactor k varies with the flow rate ratio such as $k \sim \varphi^{1/2}$ [Fig. 6(c)(inset)]. When the length L_P/h is plotted against $\varphi^{1/2}Q_T^{2/3}$, data collapses together onto a master curve defined as $L_P/h = 2.1 \varphi^{1/2} Q_T^{2/3}$ [Fig. 6(c)]. Using a similar approach, a restricted homogeneous expression of the form $L_P/h = 1.7 \, \varphi^{1/2} Q_T^{2/3}$ is found for the nanoemulsion. Overall, the persistence length can be expressed as:

$$\frac{L_{\rm P}}{h} = \varphi^{1/2} \left(\frac{Q_{\rm T}}{Q_{\rm P}} \right)^{2/3},\tag{5}$$

where Q_P is the persistence flow rate depending on fluid properties, such as $Q_{P,E} = 0.32 \ \mu l/min$ for the microscale emulsion and $Q_{P,N} = 0.45 \ \mu l/min$ for the nanoemulsion.

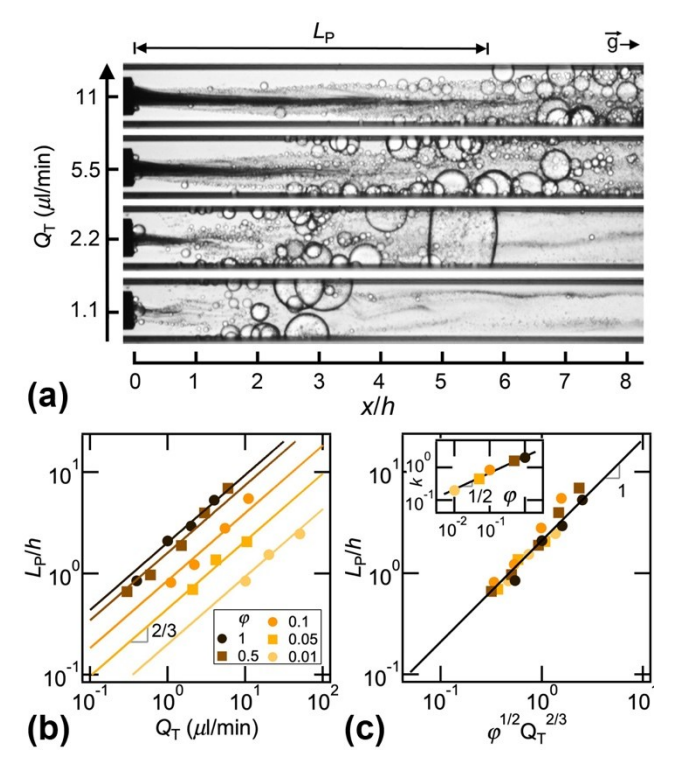


Fig. 6 Thread persistence length L_P in the dissolution regime. (a) Micrographs of dissolving threads of microscale emulsion in isopropanol solvent (downward orientation) at fixed $\varphi = 0.1$ where $Q_1 = 0.1$, 0.2, 0.5, and 1 μ l/min (from bottom to top). (b) Iso- φ evolution of normalized length L_P/h as a function of total flow rate Q_T . Solid lines: $L_P/h = kQ_T^{2/3}$. (c) Scaled persistence length L_P/h compared to scaling $\varphi^{1/2}Q_T^{2/3}$. Solid line: eq. (5) . Inset: Evolution of prefactor k as a function of flow rate ratio φ . Solid line: $k = 2.1 \varphi^{1/2} (\min/\mu l)^{3/2}$.

As the stable thread diameter scales as $\varepsilon/h \sim \varphi^{1/2}$, our results show that for a given Q_T , L_P is roughly proportional to the diameter ε as thicker threads maintain longer structural integrity compared to smaller threads when co-flowing with the solvent. Incidentally, the thread persistence length L_P also provides an indicator of the transition from the dissolving to the diffusive regime as assuming a fixed $L_P/h \sim 10$, corresponding to the field of view, at the transition, yields a scaling of the form $\varphi \sim Q_T^{-4/3}$ for the transition curve in the $\varphi - Q_T$ flow maps, which is in qualitative agreement with previous scaling $\varphi \sim Q_T^{-2}$. While this initial finding is suggestive, we recognize that more work would be required to refine regime transition criteria of complex time-evolving emulsion threads in miscible solvents.

Another important aspect of emulsion thread alteration processes in solvents is observed in the diffusive regime, *i.e.*, when threads traverse the initial field of view near the fluid contactor with significant lateral enlargement (Fig. 7). Threads made of microscale emulsion with $\langle a \rangle \sim 0.58~\mu m$ and those made of nanoemulsion with $\langle a \rangle \sim 51$ nm appear visually different on micrographs, For the emulsion, droplets grow gradually along the thread, diffuses to the outer phase fluid L_2 , and condensate at the channel walls [Fig. 7(c)]. As such, larger droplets stick to the channel walls, accumulate detached droplets, and eventually detach from the wall to flow downstream. This process produces an apparent large envelope around the thread indicating significant diffusive processes. For the nanoemulsion, while it is difficult to directly visualize individual droplets, the thread displays rough surface upstream and become blurry downstream with an enlarged measured diameter $\mathcal{E}h$ [Fig. 7(b)]. In both cases, the thread diameter $\mathcal{E}h$ can be measured at moderate Q_T and compared to the stable thread diameter \mathcal{E}_0 , which solely depends on φ at large Q_T . Our previous work on the swelling of diffusive threads made of pure silicone oil using hydrodynamic focusing in microchannels⁴⁴ yields a simple method for analyzing the relationship between $\mathcal{E}h$ and Q_T at various φ using bounded functions of the form:

$$\frac{\varepsilon}{h} = 1 - \left[\frac{1}{1 - \varepsilon_0 / h} + \left(\frac{Q_T}{Q_C} \right)^{-1.5} \right]^{-1}, \tag{6}$$

where the critical flow rate $Q_{\mathbb{C}}$ is the only fitting parameter for a given fluid pair.

Another useful aspect of this approach is the possibility of relating Q_C to the diffusion coefficient D using dynamic similarity and reference fluids. Therefore, we conduct experiments with pure silicone oil having a diffusion coefficient D in downward coaxial microchannels and examine the evolution of $\mathcal{E}h$ as a function of Q_1 [Fig. 7(a)]. As can be seen on the figure, the evolution of the diameter for iso- φ curves is well fit with eqn (6) using the identity $Q_1 = Q_T/(1+\varphi^{-1})$ and eqn (1) for the thread diameter. The critical flow rate found for the oil corresponds to $Q_C = Q_0 = 7 \mu l/min$ for a diffusion coefficient estimated at $D_0 = 9.6 \times 10^{-10}$ m²/s. ⁴⁶ Data for the fluid pair nanoemulsion and isopropanol, is analyzed in a similar fashion and well fit with a critical flow rate $Q_N = 10 \mu l/min$ [Fig. 7(b)]. Meanwhile, the critical flow rate for the microscale emulsion and isopropyl alcohol is found at $Q_E = 25 \mu l/min$ [Fig. 7(c)]. Diffusive core-annular flows are often treated using a Péclet number Pe = Vh/D, which compares convective and diffusive transport in confined flow systems. Assuming a constant Pe for the diffusive-convective transition of miscible threads, the critical flow rate scales as $Q_C \sim Dh$, which enables one to estimate the effective diffusion coefficients of colloidal dispersions of droplets in miscible solvent such as $D_N = D_0 Q_N/Q_0 \approx 1.37 \times 10^{-9}$ m²/s and $D_E \approx 3.42 \times 10^{-9}$ m²/s. While the use of a reference fluid permits direct estimation of diffusion coefficients D, the ratio of critical flow rates found in the diffusive regime between emulsion and nanoemulsion $Q_E/Q_N \approx 2.5$ is comparable to the ratio of critical flow rates found for the dissolution-diffusive regime transition

 $Q_{\rm V,E}/Q_{\rm V,N} \approx 2.4$ highlighting a consistent trend in diffusive behavior between colloidal dispersion of droplets having various < a >.

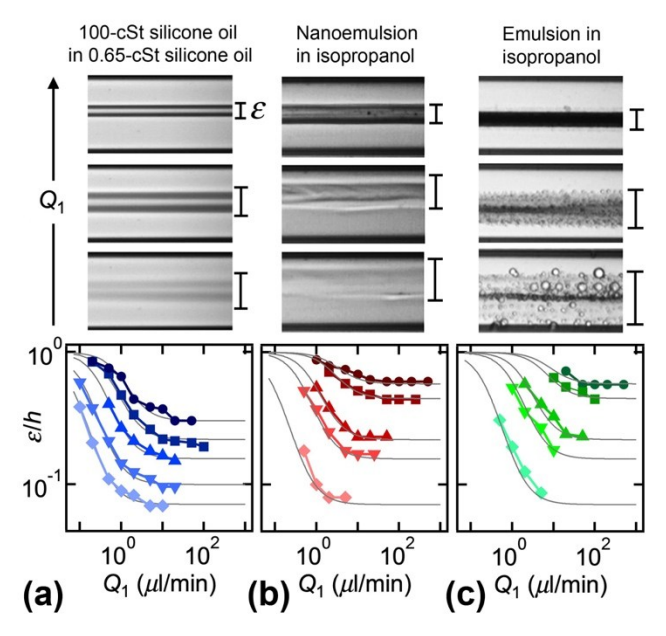


Fig. 7 Diffusive thread diameter at x/h = 10. Downward configuration, flow rates in μ l/min (a) Top: micrographs of 100-cSt silicone oil in 0.65-cSt silicone oil at $\varphi = 10^{-1}$ with $Q_1 = 1$, 5, and 50. Bottom: Evolution of normalized diameter ε/h as a function of Q_1 , $\varphi = 0.2$ (\bullet), 0.1 (\blacksquare), 0.05 (\blacktriangle), 0.02 (\blacktriangledown), and 0.01 (\bullet). Iso- φ lines: Eqn (6) with $Q_C = 7$. (b) Top: micrographs of nanoemulsion in isopropanol at $\varphi = 10^{-1}$ with $Q_1 = 1$, 2, and 50. Bottom: ε/h vs. Q_1 , $\varphi = 1$ (\bullet), 0.5 (\blacksquare), 0.1 (\blacktriangle), 0.05 (\blacktriangledown), and 0.01 (\bullet). Iso- φ lines: Eqn (6) with $Q_C = 10$ (c) Top: micrographs of emulsion in isopropanol at $\varphi = 5 \times 10^{-2}$ with $Q_1 = 1$, 2, 100. Bottom: ε/h vs. Q_1 , $\varphi = 1$ (\bullet), 0.5 (\blacksquare), 0.1 (\blacktriangle), 0.05 (\blacktriangledown), and 0.01 (\bullet). Iso- φ lines: Eqn (6) with $Q_C = 25$.

Finally, we examine the intriguing morphologies associated with the diffusion of nanoemulsion threads in solvents at low flow rates Q_T . While the regime of small threads $\varepsilon/h \ll 1$ is of interest to characterize dissolution processes, flow patterns associated with larger threads $\varepsilon/h \ll 1$ display remarkable features. In particular, for low Q_T , the long residence time of both inner and outer fluids facilitates the mixing of emulsion and solvent, and complex droplet coalescence processes are observed. For instance, Figure 8(a) displays a time series of micrographs showing the evolution of a droplet formed through solvent interaction with the nanoemulsion in the upward configuration. Image processing techniques are implemented to document the droplet spatial growth d/h [Fig. 8(b)] and change in lateral position y/h [Fig. 8(c)] along the flow direction x/h and provide insights into complex fluid rearrangement processes developing along the core of larger threads. It is shown that as the droplet travels from $x/h \sim 2$ to 9, the size increases from $d/h \sim 0.05$ to 0.25 and the droplet does not follow the mean flow path as it moves downstream. In addition to the formation of discrete structures, such as droplets, straight and sinuous streams of conjugate fluids appear near the edge of large threads and complex chevron-like instabilities are

observed in the thin intercalating film near the walls at relatively large flow rate ratios φ [Fig. 8(d)]. Overall, nanoemulsion and solvent multiphase flows at large concentration present a vast collection of intricated flow patterns, and more work is required to fully unravels thick thread dynamics and destabilization processes at long time scales.

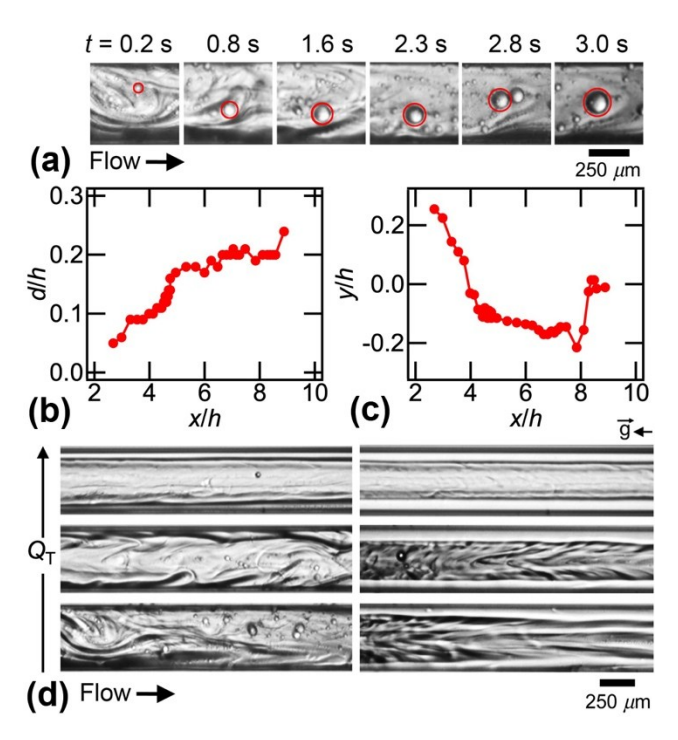


Fig. 8 Upward flow of nanoemulsion at large flow rate ratios φ . Flow rates in μ l/min. (a) Time-series of micrographs showing the evolution of a meandering droplet in the droplet reference frame for large thread diameter, $Q_1 = 5$ and $Q_2 = 5$. (b) Evolution of droplet diameter d/h along the flow direction x/h. (c) Droplet lateral position y/h as a function of x/h. (d) Micrographs of upward injection of nanoemulsion at $\varphi = 1$ with $Q_T = 10$, 16, and 36 (left), and $\varphi = 0.3$ with $Q_T = 13$, 26, and 65 (right).

5. Conclusions

In this work, we have examined the flow behavior of nanoemulsion jets in solvents using coaxial microfluidic devices. Colloid dispersions made of oil droplets in aqueous SDS solutions are centrally injected in a sheath of isopropyl alcohol, which is miscible with both oil and water phases. As a result, the solvent dissolves the emulsion through a progression of droplet growth and coalescence processes across various time-scales. We manipulate the residence time of nanoemulsions in small fluidic passages through wide variations of flow rates Q_1 and Q_2 and examine the cross-over between dissolving, diffusive, and stable thread regimes. To decorrelate gravitational and diffusive effects at low velocities, we examine three microchannel orientations, including horizontal, upward, and downward. This approach enables us to map and systematically characterize numerous flow regimes of interest to the microfluidic processing of soft matter.

We find, in particular, that the stable thread diameter ε_0 remains unchanged across all orientations and only depends on the flow rate ratio $\varphi = Q_1/Q_2$ at large total flow rate $Q_T = Q_1 + Q_2$. This feature provides a reference length for the study of dissolving and diffusive flows at low Q_T . We first examine the role of the channel orientation on the flow of nanoemulsion in solvent and compare the horizontal and vertical downward configurations. We find that due to differences in fluid densities, the gravitational regime becomes preponderant in horizontal channels with a thread progressively drifting toward the channel walls over a distance L_G/h at low velocities, which hinders the study of pure diffusive effects in core-annular microflows. By contrast, in the downward configuration, the emulsion thread remains surrounded by the solvent at moderate Q_T , which permits examination of diffusive colloidal thread behavior. The study of transition curves on φ - Q_T diagrams for the dissolving and diffusive regimes in the downward configuration reveals differences in critical flow rates Q_V between nanoemulsion and microscale emulsion for the regime transition $\varphi \sim (Q_T/Q_V)^{-2}$. This finding shows that larger threads are more resistant to dissolution and highlights the relationship between critical flow rates and diffusive fluid properties since larger Q_V indicates larger effective diffusion coefficient D between the colloid and the solvent. We also examine the evolution of the persistence length L_P/h in the dissolving regime based on a simple scaling relationship between φ and Q_T to decorrelate the influence of the thread size with φ and the role of the diffusive flux with Q_T on the melting of emulsion threads.

In the diffusive regime, we measure the enlargement of thread diameter ε/h downstream from the fluid contactor at $x/h \sim 10$ and show that bounded functions based on φ , Q_T , and a critical flow rate Q_C depending on fluid pair provide a means to model experimental data. Using silicone oils as reference fluid pair together with dynamic similarity arguments based on the Péclet number, we estimate the effective diffusion coefficient D of nanoemulsion and microscale emulsion in isopropanol solvent. Finally, we inspect destabilization regimes in the upward configuration and discuss droplet coalescence and various aspects of thick nanoemulsion thread morphology.

Future investigations could focus on examining the influence of various surfactant types on regime transitions and interrogate the role of solvent miscibility, for instance with higher molecular weight alcohols, on flow regimes. Work is also required to advance theoretical and numerical modeling of dissolving and diffusive flow regimes and clarify the relationship between interfacial flow processes and physicochemical properties of dispersions. It would be helpful to further inquire into the phenomenon of coalescence cascade triggered by solvent penetration in colloidal media and develop microfluidic techniques to control degradation processes of soft materials in confined microenvironments. Overall, this work reveals a variety of microflow regimes between nanoscale emulsions and organic solvent and opens up new routes to expand the domain of microfluidic postprocessing of complex fluids.

Conflicts of interest

The authors declare no competing financial interest.

Data availability

The raw data supporting this article consist of a large collection of digital movies of size $\sim 10^2$ GB, which are stored and archived on computers and hard-drives. All data are available to interested parties.

Acknowledgements

This material is based upon work supported in part by the National Science Foundation under Grand No. CBET-2223988. TGM and YX thank UCLA for support.

References

- 1 K. Meleson, S. Graves, and T. G. Mason, Soft Materials, 2004, 2, 109.
- 2 F. Leal-Calderon, V. Schmitt, and J. Bibette, Emulsion Science: Basic Principles. Springer: New York, 2007.
- 3 A. Gupta, H. B. Eral, T. A. Hatton, and P. S. Doyle, Soft Matter, 2016, 12, 2826.
- 4 T. Krebs, K. Schroen, and R. Boom, Lab Chip, 2012, 12, 1060.
- 5 A. Nowbahar, K. A. Whitaker, A. K. Schmitt, and T.-C. Kuo, Energy Fuels, 2017, 31, 10555.
- 6 T. Cubaud, Phys. Rev. Fluids, 2023, 8, 104201.
- 7 T. G. Mason, J. N. Wilking, K. Meleson, C. B. Chang, and S. M. Graves, *J. Phys.: Condens. Matter*, 2006, 18, R635.
- 8 N. Anton, J.-P. Benoit, and Saulnier, J. Controlled Release, 2008, 128, 185.
- 9 C. Solans and I. Solé, Current Opinion in Colloids & Int. Sci., 2012, 12, 246.
- 10 D. J. McClements, Soft Matter, 2012, **8**, 1719.
- 11 T. Delmas, H. Piraux, A. C. Couffin, I. Texier, F. Vinet, P. Poulin, M. E. Cates, and J. Bibette, *Langmuir*, 2011, 27, 1683.
- 12 H. S. Kim and T. G. Mason, Adv. Colloid Interface Sci., 2017, 247, 397.
- 13 L. Pavoni, D. R. Perinelli, G. Bonacucina, M. Cespi, and G. F. Palmieri, Nanomaterials, 2020, 10.
- 14 T. M. Squires and S. R. Quake, Rev. Mod. Phys., 2005, 77, 977.
- 15 M. Hashimoto, P. Garstecki, H. A. Stone, and G. M. Whitesides, Soft Matter, 2008, 4, 1403.
- 16 T. Gu, E. W. Q. Yeap, A. Somasundar, R. Chen, T. A. Hatton, and S. A. Khan, Lab Chip, 2016, 16, 2694.
- 17 H. M. Xia, J. W. Wu, J. J. Zheng, J. Zhang, and Z. P. Wang, Lab Chip, 2021, 21, 1241.
- 18 P. A. Zhu and L. Q. Wang, Chem. Rev., 2021, 122, 7010.

- 19 P. Guillot, A. Colin, and A. Ajdari, *Phys. Rev. E*, 2008, **78**, 016307.
- 20 R. Seemann, M. Brinkmann, T. Pfohl, and S. Herminghaus, Rep. Prog. Phys., 2011, 75, 016601.
- 21 N. Bremond and J. Bibette, *Soft Matter*, 2012, **8**, 10549.
- 22 L. L. A. Adams, T. E. Kodger, S.-H. Kim, H. C. Shum, T. Franke, and D. A. Weitz, *Soft Matter*, 2012, **8**, 10719.
- 23 S. L. Anna, Annu. Rev. Fluid Mech., 2016, 48, 285.
- 24 K. Doufène, C. Tourné-Péteilh, P. Etienne, and A. Aubert-Pouëssel, Langmuir, 2019, 35, 12597.
- 25 T. P. Santos, C. M. Cejas, R. L. Cunha, and P. Tabeling, Soft Matter, 2021, 17, 1821.
- 26 T. Dinh and T. Cubaud, Langmuir, 2021, 37, 724.
- 27 B. Morin, Y. Liu, V. Alvarado, and J. Oakey, *Lab Chip*, 2016, **16**, 3074.
- 28 D. D. Joseph and Y. Y. Renardy, Fundamentals of Two-Fluid Dynamics. Part II: Lubricated Transport, Drops and Miscible Liquids Springer-Verlag: New York, 1993.
- 29 B. Selvam, S. Merk, R. Govindarajan, and E. Meiburg, J. Fluid. Mech., 2007, 592, 23.
- 30 S. Tottori and S. Takeuchi, *RSC Adv.*, 2015, **5**, 33691.
- 31 D. Salin and L. Talon, *J. Fluid Mech.*, 2019, **865**, 743.
- 32 V. Jayaprakash, M. Costalonga, S. Dhulipala, and K. K. Varanasi, Adv. Healthcare Mater., 2020, 9, 2001022.
- 33 C. Chung, D. Choi, J. M. Kim, K. H. Ahn, and S. J. Lee, Microfluid Nanofluid, 2010, 8, 767.
- 34 A. Duboin, R. Middleton, F. Malloggi, F. Monti, and P. Tabeling, Soft Materials, 2013, 9, 3041.
- 35 J. K. Nunes, H. Constantin, and H. A. Stone, Soft Matter, 2013, 9, 4227.
- 36 S. Gosh, G. Das, K. Prasanta, and K. Das, Eur. Phys. Lett., 2016, 115, 44004.
- 37 O. du Roure, A. Lindner, E. N. Nazockdast, and M. J. Shelley, Ann. Rev. Fluid Mech., 2019, 51, 539.
- 38 V. K. Gowda, C. Rydefalk, L. D. Söderberg, and F. Lundell, Phys. Rev. Fluids, 2021, 6, 114001.
- 39 L. Cai, J. Marthelot, and P.-T. Brun, Proc. Nat. Acad. Sci., 2019, 116, 22966.
- 40 T. Cubaud, B. Conry, X. Hu, and T. Dinh, Phys. Rev. Fluids, 2021, 6, 094202.
- 41 T. Dinh, Y. Xu, T. G. Mason, and T. Cubaud, Phys. Rev. E, 2023, 107, 015101.
- 42 J. Israelachvili, Intermolecular and surface forces. Academic Press: Amsterdam, 1991.
- 43 Q. Cao, A. L. Ventresca, K. R. Sreenivas, and A. K. Prasad, Canadian J. of Chem. Eng., 2003, 81, 913.
- 44 T. Cubaud, Phys. Rev. Lett., 2020, 125, 174502.
- 45 J. Crank, The Mathematics of Diffusion. Oxford University Press Inc.: New York, 1975.
- 46 N. Rashidnia, R. Balasubramaniam, J. Kuang, P. Petitjeans, and T. Maxworthy, *Int. J. Thermophys.*, 2001, **22**, 547.